Designing, Characterization, DFT, Biological Effectiveness, and Molecular Docking Analysis of Novel Fe(III), Co(II), and Cu(II) Complexes Based on 4-Hydroxy-2*H*-pyrano[3,2-*c*]quinoline-2,5(6*H*)-dione

Mai M. Khalaf, Hany M. Abd El-Lateef,* Mohamed Gouda, Antar A. Abdelhamid, Amer A. Amer, and Aly Abdou*

Cite This: *ACS Omega* 2024, 9, 6466−6481

Read Online

ACCESS | Metrics & More | Article Recommendations | Supporting Information

ABSTRACT: The main target of the current framework is the designing and synthesizing of novel iron(III), cobalt(II), and cupper(II) complex compounds emanating from bioactive nucleus, 4-hydroxy-2H-pyrano[3,2-*c*]quinoline-2,5(6H)-dione ligand, to enhance comprehension as potential antibacterial, antifungal, and antioxidant alternatives by means of using DFT calculations and molecular docking investigation. Thus, the new complexes had been synthesized and characterized using various analytical techniques, including elemental analysis, infrared spectroscopy, mass spectrometry, UV spectroscopy, conductivity, and magnetic testing, as well as thermal analysis. The 4-hydroxy-2H-pyrano[3,2-*c*]quinoline-2,5(6H)-dione ligand exhibits monobasic bidentate OO donor properties toward the metal core, as shown by its infrared spectroscopic characteristics. The use of thermal analysis techniques allows for the identification and characterization of water molecules present inside the complexes, as well as the determination of their distribution patterns. The molecular structures of free ligand and its metal complex compounds have been verified through the use of density functional theory (DFT) simulations. These simulations also provide a valuable understanding of the quantum chemical characteristics associated with these structures. *In vitro* experiments were conducted to evaluate the antioxidant, antibacterial, as well as antifungal and the properties of the free ligand and its corresponding complex compounds. DATA revealed that synthesized metal complex compounds have heightened biological efficacy as related to the unbound ligand. Furthermore, molecular docking analysis was done to understand the interactions between the studied compounds and proteins derived from *Escherichia coli* (pdb ID: 2vf5), *Aspergillus flavus* (pdb ID: 3cku), and humans (pdb ID: 5IJT), which are considered to be significant in drug design. Lastly, a correlation between *in vitro* efficacies with molecular docking data was done and analyzed.

1. INTRODUCTION

Quinoline-dione complexes are a class of compounds that have attracted significant attention recently due to their various biological effectiveness and potential applications in various fields. Quinoline-dione is a heterocyclic ring system that consists of a quinoline moiety fused with a 1,4-diketone group. 1-Benzopyridine is an advantaged scaffold that shows as a significant construction subject for the enhancement of novel drug compounds, as it exhibits a wide range of biological effectiveness, such as bactericidal, antifungal, antimalarial, anthelmintic, anticonvulsant, cardiotonic, anti-inflammatory, and analgesic activities.[1] Quinoline-dione can act as a bidentate ligand and form metal complexes with various transition and lanthanide metals.[2] These metal complexes can exhibit enhanced or novel biological properties compared to the free ligands, as well as interesting analytical applications.[3]

Some of the reported biological activities of quinoline-dione complexes are antibacterial activity: quinoline-dione complexes have shown potent antibacterial activity against various Gram-positive and Gram-negative bacteria, such as *Staphylococcus aureus*, *Escherichia coli*, *Pseudomonas aeruginosa*, and *Bacillus subtilis*. The antibacterial activity of these complexes may be attributed to their ability to interfere with the bacterial DNA gyrase enzyme, which is essential for DNA replication and transcription.[4] Antifungal activity: quinoline-dione complexes have also demonstrated antifungal effectiveness against various

fungi, such as *Candida albicans*, *Aspergillus niger*, and *Fusarium oxysporum*. The antifungal activity of these complexes may be related to their ability to inhibit the fungal cytochrome P450 enzyme, which is involved in the biosynthesis of ergosterol, a vital component of the fungal cell membrane.[4] Antivirulence activity: Quinoline-dione complexes have been found to inhibit the virulence factors of pathogenic bacteria, such as biofilm formation, quorum sensing, and toxin production. These virulence factors are responsible for the persistence and severity of bacterial infections. By inhibiting these factors, quinoline-dione complexes can reduce the bacterial pathogenicity and enhance the efficacy of conventional antibiotics.[5] Anticancer activity: Quinoline-dione complexes have exhibited anticancer activity against various cancer cell lines, such as breast tumor, lung tumor, colon cancer, and leukemia. The anticancer effectiveness of these complexes may be mediated by their ability to persuade apoptosis (programmed cell death), arrest cell cycle progression, inhibit angiogenesis (blood vessel formation), and modulate signaling pathways involved in cancer development and progression.[4]

In summary, quinoline-dione complexes are promising candidates for the development of new drugs with multiple therapeutic targets and applications. Further research is needed to explore the structure−activity relationships, mechanisms of action, pharmacokinetics, and toxicity profiles of these complexes. Consequently, the objective of the research is synthesis and structural characterization of three novel Fe(III) (**C2**), Co(II) (**C3**), and Cu(II) (**C4**) complexes exhibiting bioactive characteristics, based on 4-hydroxy-2H-pyrano[3,2-*c*]quinoline-2,5(6H)-dione ligand (**C1**). Our research endeavors to yield a new category of compounds based on bioactive moiety, that, because of their straightforward synthesis and therapeutic efficacy, have promising prospects for addressing bacterial amd fungal infections.

The manuscript introduces a novel approach involving the fabrication and synthesis of distinct Fe(III) (**C2**), Co(II) (**C3**), and Cu(II) (**C4**) complex compounds. These complexes are derived from a bioactive moiety, specifically the 4-hydroxy-2H-pyrano[3,2-*c*]quinoline-2,5(6H)-dione ligand (**C1**), known for its simplicity and ease of synthesis. The primary objective is to enhance our understanding of their antimicrobial properties and therapeutic efficacy. To achieve this, DFT calculations and molecular docking studies, measured pivotal in current research, are employed. The investigation includes the design and characterization of the novel metal complexes [Fe(III) (**C2**), Co(II) (**C3**), and Cu(II) (**C4**)], along with an in-depth exploration of their *in vitro* and *in silico* antimicrobial and antioxidant activities. The study extends further to scrutinize the geometric structures of the compounds through the application of the DFT calculations. Additionally, in silico molecular docking experiments shed light on the interactions between the synthesized compounds and key enzymes, such as glucosamine-6-phosphate synthase, and urate oxidase from *Aspergillus flavus* (3cku), in addition to the oxidized form of human peroxiredoxin 2 (5IJT), crucial in the realm of drug design. The manuscript concludes with a comprehensive analysis and discussion that correlates the *in vitro* effectiveness findings with the DFT and molecular docking results.

2. METHODOLOGY

2.1. Synthesis. *2.1.1. Materials.* All constituents were of the utmost purity, meeting either the highest available standards or conforming to analytical reagent (AR) grade.

Aniline, diethyl malonate, and iron(III) chloride hexahydrate (FeCl$_3$·6H$_2$O), cobalt(II) chloride hexahydrate (CoCl$_2$·6H$_2$O), and copper(II) chloride dihydrate (CuCl$_2$·2H$_2$O) are just a few examples obtained from Sigma-Aldrich. BDH supplied spectroscopically pure organic solvents, including but not limited to ethanol, DMF, and acetonitrile.

*2.1.2. Preparation of **C1** Ligand.* The 4-hydroxy-2H-pyrano[3,2-*c*]quinoline-2,5(6H)-dione (**C1**) ligand was synthesized as described before,[6−8] as illustrated in Scheme 1. The detailed methodology was listed in the Supporting Information, S.1.

Scheme 1. Synthesis Procedures of the C1 Ligand
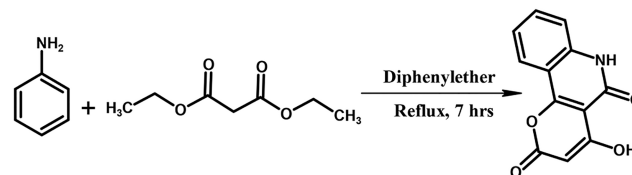
*2.1.3. Preparation of the Fe(III) (**C2**), Co(II) (**C3**), and Cu(II) (**C4**) Complexes.* Synthesis of the **C2**, **C4**, and **C3** compounds were carried out through heating a mixture of C1 ligand (2.0 mmol, 10 mL ethyl alcohol), with the respective Fe(III), Co(II), or Cu(II) salt (2.0 mmol, 10 mL H$_2$O). The reaction mixture was continuously stirred and refluxed at 79 °C for a duration of 12 h. After the completion of the reaction, the resulting product was filtered and washed with a water−ethanol mixture (1:2 ratio). The isolated product underwent a drying process and was subsequently subjected to recrystallization. The yield and thermal properties of the product were then measured, as illustrated in Scheme 2.

2.2. Characterization. The Supporting Information, S.2. characterization provides a comprehensive list of the tools employed for the characterization of both **C1** and its corresponding complexes, namely **C2**, **C4**, and **C3**. Detailed information on characterization techniques is made available to ensure transparency and reproducibility in the experimental procedures.

2.3. DFT Calculations. Geometry optimization of **C1** and its agreeing **C2**, **C4**, and **C3** had been done via the DFT/B3LYP[9] in combination with the LANL2DZ[10] for metal atoms, and the 6-311 (d,p)[11] basis set for the other atoms, using Gaussian 09w.[12] The quantum chemical characteristics were obtained by using the highest occupied molecular orbital (HOMO) and lowest unoccupied molecular orbital (LUMO) of **C1** and its corresponding **C2**, **C4**, and **C3**. The parameters encompassed in this context consist of energy gap (ΔE); $\Delta E = E_{LUMO} - E_{HOMO}$.[13] Electronegativity, represented as χ, is determined as $\chi = (IP + EA)/2$. The chemical potential, denoted as CP, is the negative value of the electronegativity (CP = $-\chi$). Chemical hardness (η) and softness (σ): $\eta = (IP - EA)/2$, $\sigma = 1/2\eta$, respectively.[14] The electrophilicity index, ω, and nucleophilicity index, Nu, are determined as $\omega = (CP^2)/(2\eta)$, and Nu = $1/\omega$, respectively.[15] In this context, the symbol IP and EA are the ionization potential (IP = $-E_{HOMO}$) and the electron affinity (EA = $-E_{LUMO}$), respectively.[16]

2.4. *In Vitro* Bioactivity Exploration. *2.4.1. Antimicrobial Activity.* In order to estimate the antimicrobial effectiveness of all compounds under scrutiny, *in vitro* agar diffusion assays were employed.[17] These assays were designed to assess the impact of the investigated compounds on a diverse array of

Scheme 2. Synthesis Steps of the C2, C4, and C3 Complexes
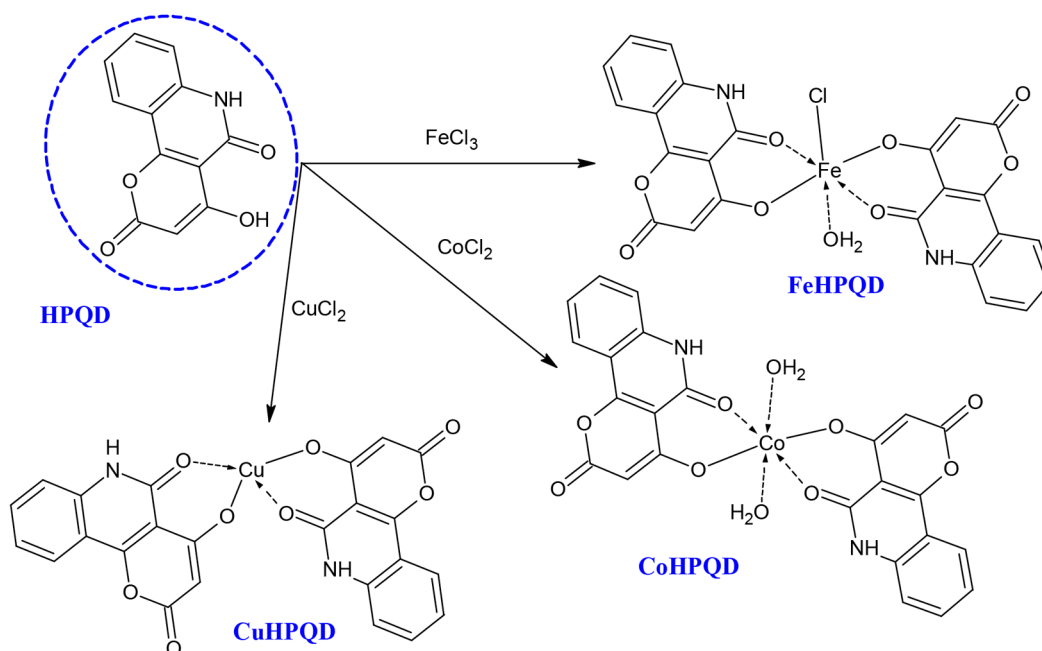
bacterial and fungal species, including *Escherichia coli*, *Pseudomonas aeruginosa*, *Bacillus cereus*, *Staphylococcus aureus*, *Aspergillus flavus*, *Candida albicans*, and *Trichophyton rubrum*. The experimental setup allowed for a comprehensive investigation into the potential antimicrobial properties of the compounds against both bacterial and fungal strains. The antibacterial and antifungal activity was measured at the same concentration of these compounds of 100 mM using DMSO as a solvent. The measurement of the zone of inhibition (ZI) around the disc was conducted in millimeters in order to assess the antibacterial effectiveness. Furthermore, the efficacy of the commonly prescribed antibiotic Ciprofloxacin was evaluated using a similar methodology to assess its effectiveness against the aforementioned pathogens. The % activity index was obtained as $\% = (ZI_{test}/ZI_{standard}) \times 100$, where ZI_{test} is the ZI of the test medication, and $ZI_{standard}$ is the ZI of the standard, herein is Ciprofloxacin.[18,19]

The calculation was conducted in order to evaluate and contrast the antibacterial and antifungal effectiveness of the components being investigated with the established antibiotic Ciprofloxacin. Ciprofloxacin was used as the standard for biological application as it is used to treat various bacterial infections, such as those affecting the skin, lungs, bones, joints, urinary tract, and gastrointestinal tract. It can also be used to prevent or treat anthrax and plague exposure.[20] Also, it has a broad spectrum of effectiveness against many types of bacteria, having Gram-positive and Gram-negative bacteria, anaerobes, and some atypical bacteria.[20] Ciprofloxacin may be preferred over other antibiotic drugs for biological applications because of its high potency, low resistance rate, good tissue penetration, and oral availability.[20]

The minimum inhibitory concentration (MIC, μM) can be defined as the lowest substance concentration, which stops detectable *in vitro* growth of bacteria or fungi. The MIC was calculated by testing a range of descending concentration, down to 10 μM, and utilizing the lowest concentration at which no inhibition activity was seen as the MIC, μM.

All the *in vitro* antimicrobial activity experiments were repeated 3 times, and the results were taken as the average $\pm$ standard deviation.

2.4.2. Antioxidant Activity. The antioxidant behavior of the **C1** and its corresponding **C2**, **C4**, and **C3** have been assessed using the DPPH test. The antioxidant activity via DPPH radical-scavenging activity had been evaluated according to the previously reported methodology[21] with slight modifications. A comprehensive and detailed outline of the methodology employed for antioxidant activity assessment has been provided in the Supporting Information, specifically outlined in Section S.3.

The concentration at which inhibitory is lowered by 50% (IC_{50}) was determined. The studies were performed in triplicate, using ascorbic acid as the reference component.[22] There are different tools or programs that can be used to calculate the IC_{50} value, which is the concentration of an inhibitor that reduces the activity of an enzyme or a binding reaction by 50%. One of the most common methods is to use a four-parameter logistic regression model, which fits the data to a sigmoidal curve and estimates the IC_{50} value from the equation. The used one is https://www.aatbio.com/tools/ic50-calculator.

All the *in vitro* antioxidant activity experiments were repeated 3 times, and the results were taken as the average $\pm$ standard deviation.

2.5. Molecular Docking. To establish a correlation between the *in vitro* biological data and binding affinity of the inhibitors, molecular docking was performed against the target protein.[23,24] During the process of docking two molecules, substrate and its target receptor active site, computational algorithm can be employed to ascertain the most favorable three-dimensional configuration that maximizes their alignment.[25] Molecular docking is an algorithmic approach used in computational chemistry to forecast the affinity and binding capability of two molecules.[26,27]

To explore the therapeutic potential of the components, molecular docking analyses were performed utilizing the MOE

Table 1. Characterization Data of the Synthesized Compounds

	(C1)	(C2)	(C3)	(C4)
color	yellow	bright violet	reddish-brown	greenish-blue
yield (%)	57	82	87	88
mp (°C)	>300	>300	>300	>300
molecular formula (MW)		$[Fe((\mathbf{1}))_2(Cl)H_2O]\cdot 3H_2O$	$[Co((\mathbf{1}))_2(H_2O)_2]\cdot 2H_2O$	$[Cu((\mathbf{1}))_2]\cdot 2H_2O$
	$C_{12}H_7NO_4$ (229)	$C_{24}H_{20}ClFeN_2O_{12}$ (619)	$C_{24}H_{20}CoN_2O_{12}$ (587)	$C_{24}H_{16}CuN_2O_{10}$ (556)
elemental analysis found (calc) %				
C	62.97 (62.89)	46.31 (46.51)	49.27 (49.08)	51.36 (51.85)
H	3.01 (3.08)	3.51 (3.25)	3.18 (3.43)	2.55 (2.90)
N	6.09 (6.11)	4.22 (4.52)	4.95 (4.77)	5.29 (5.04)
M	–	9.47 (9.01)	9.84 (10.03)	11.32 (11.43)
conductivity (DMF, 1×10^{-3} M)				
μ_v, Ω^{-1} cm^2 mol^{-1}	–	9.87	9.48	10.11
		nonelectrolyte	nonelectrolyte	nonelectrolyte

Table 2. IR Spectra Data: Calculated (Practical) of the Synthesized Compounds

	(C1)	(C2)	(C3)	(C4)
v (−OH)	3380 (3415)	3522 (3475)	3495 (3473)	3428 (3470)
v (−C=O)	1653 (1670)	1679 (1607)	1642 (1612)	1657 (1610)
v (M−O)	–	598 (577)	609 (568)	587 (572)
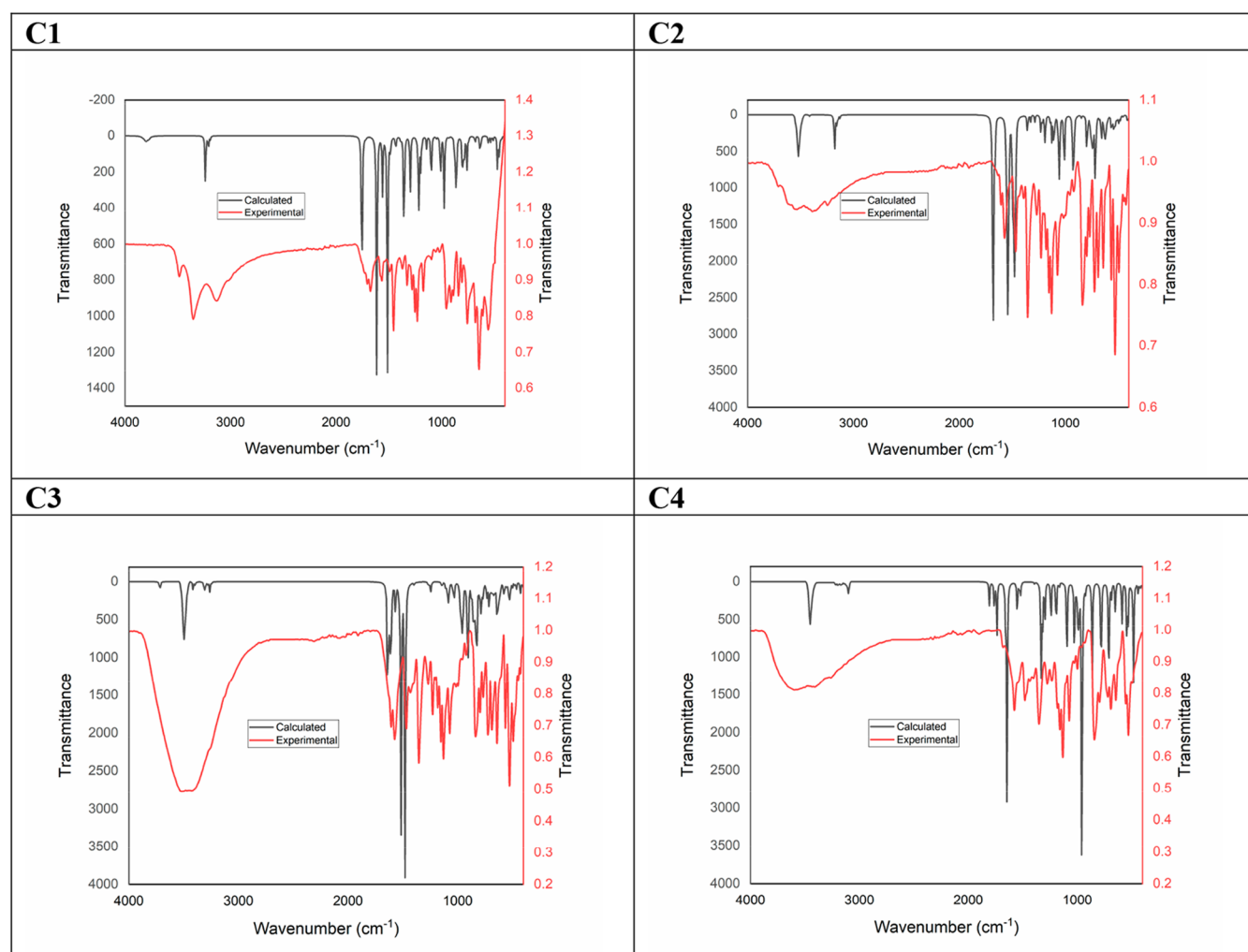
Figure 1. Calculated and experimental IR spectra of the synthesized compounds.
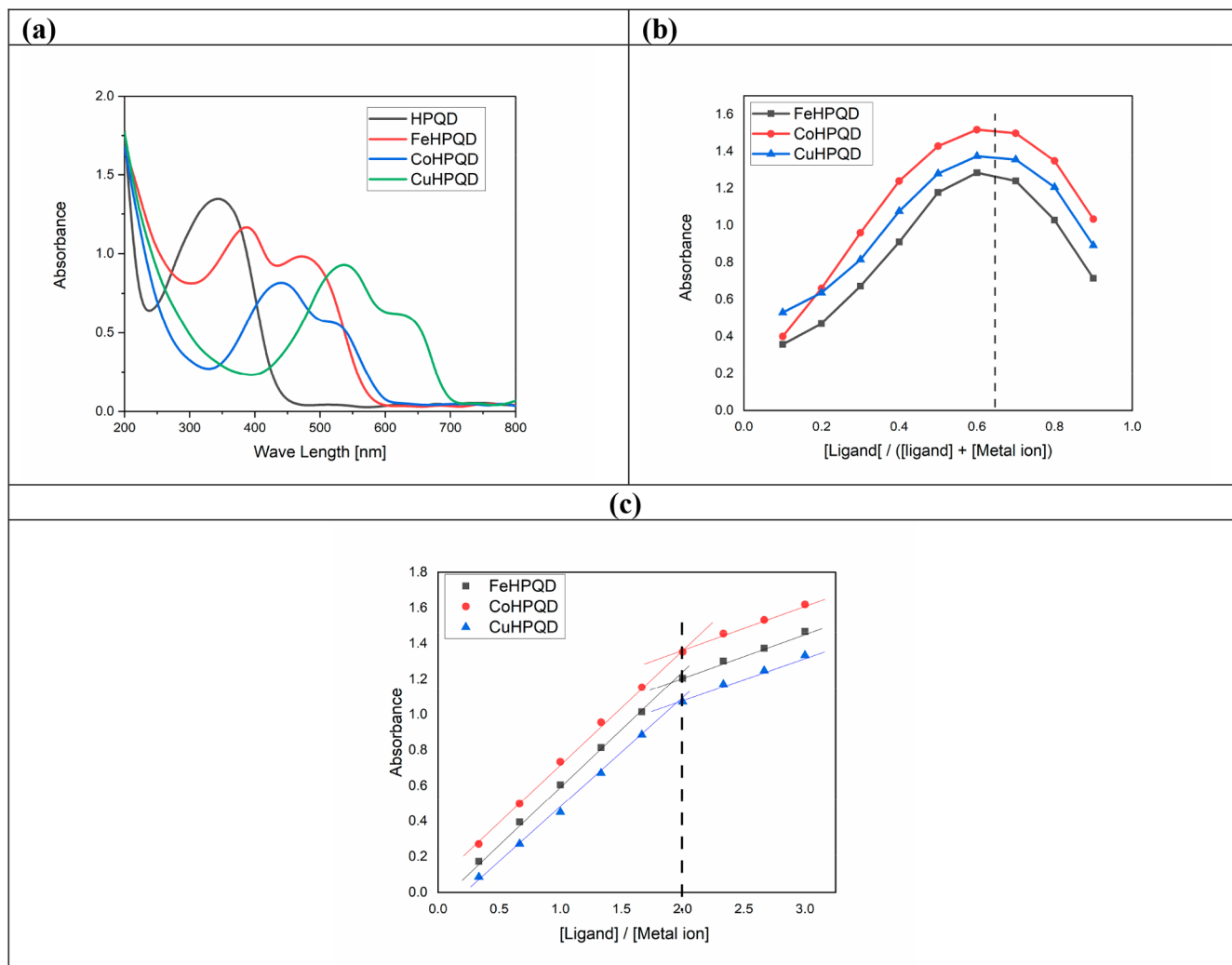
Figure 2. (a) UV−vis spectra, (b) Job's method, and (c) molar ratio method.

software.[28] The target proteins selected for docking included glucosamine-6-phosphate synthase from *Escherichia coli* (2vf5),[29] urate oxidase from *Aspergillus flavus* (3cku),[30] and the oxidized form of human peroxiredoxin 2 (5IJT).[31,32] This approach aimed to evaluate the binding strengths and effectiveness of both **C1** and its matching **C2**, **C4**, and **C3** by conducting a comparison of their docking scores and the amounts of interactions they have with the proteins that were indicated.[33] The detailed methodology and results of the molecular docking analyses are elaborated upon in subsequent sections, providing a comprehensive understanding of the molecular interactions and potential therapeutic relevance of the investigated compounds.

Leveraging the rcsb.org database, we successfully elucidated the three-dimensional structure of the target receptor protein for our study. The compounds under investigation were employed as substrates in the experimental setup. To facilitate the subsequent docking process, a dedicated mdb file had been formed for each compound, and their energies were subsequently minimized. The receptor preparation involved crucial steps, such as incorporating hydrogen atoms, defining receptor types, constraining potential energy, and exploring active pockets. Evaluation of the inhibitory potential was carried out using the exportation of docking interaction data, accompanied by the assignment of a docking score (S, kcal/

mol).[34,35] This meticulous process ensured a robust foundation for assessing the compounds' interactions with the target receptor, providing valuable insights into their inhibitory effects.

3. RESULTS AND DISCUSSION

3.1. C1 Ligand Characterization.
Structural characterization of the synthesized ligand was discussed in the Supporting Information, S.4. and Figure S.1.

3.2. C2, C4, and C3 Complexes Characterization.
3.2.1. Elemental Analysis and Conductivity Data. The investigation into the solubility and stability of **C2**, **C4**, and **C3** revealed distinctive characteristics. Notably, water insolubility was observed for the metal complex compounds, whereas solubility in DMF and acetonitrile was evident. Molar conductivity, measured in a DMF solution with a concentration of 0.001 mol/L, along with elemental analysis, was meticulously documented and presented in Table 1. Interestingly, practical elemental analyses values closely aligned with the calculated values, ensuring consistency in the results. Remarkably, the metal complexes exhibited low values of molar conductivity, as depicted in Table 1, indicative of their nonelectrolytic properties. This comprehensive characteriza-

tion sheds light on the distinct solubility profiles and conductivity behaviors of the investigated metal complexes.

3.2.2. IR Spectra. In order to gain a deeper insight into the intricate interactions between ligands and metal ions, we employed infrared spectroscopy, and the results are meticulously presented in Table 2 and Figure 1. The significant infrared (IR) bands, crucial for understanding the molecular dynamics of C1 and its corresponding **C2**, **C4**, and **C3**, have been detailed in Table 2 and visually depicted in Figure 1. Attributing these bands to the interaction of the metal ions to **C1** via the binding regions of **C1** is the explanation for their existence. At a frequency of 1670 cm^{-1}, the infrared spectrum of the free **C1** ligand displayed a unique peak, indicating the existence of the carbonyl (C=O) structure in the system. In addition, a band that could be identified at 3415 cm^{-1} was found, which is significant since it represents the hydroxyl (HO−) group. This detailed analysis sheds light on the specific vibrational modes associated with the interaction of metal ions, providing valuable insights of molecular interactions within the studied complexes. A drop in wave numbers of the C=O group bands in the infrared (IR) spectrum of the **C1** ligand was detected following its contact with the metal ion, as seen in Table 2 and Figure 1. The finding has presented empirical support for the occurrence of a coordination complex formation between the metal ion and oxygen within the C=O group. Additionally, it was noted that the metal complexes had a reduction in the vibration of the phenolic (−OH) group.[36,37] As a result, a hypothesis was postulated, proposing that the involvement of the phenolic oxygen of the **C1** is significant in the process of C−O−M bond formation subsequent to deprotonation. The cause of the wide spectral band seen at 3400 cm^{-1} in the **C1** via the **C1** was discovered to be the hydroxyl (−OH) groups found in water molecules. Table 2 and Figure 1 display the finding of one previously unreported spectral bands, referred to as M−O.[36] In accordance with the results of this experiment, the C1-ligand demonstrated the characteristics of a mononegative bivalent OO ligand. This was shown by the fact that it created coordinating contacts with the metal ion via the use of its phenolic oxygen (−OH) and −C=O moieties.

At the DFT/B3LYP[9] in combination with the LANL2DZ[10] for metal atoms, and the 6-311 (d, p)[11] for the other atoms, the vibrational frequencies (IR) of the investigated compounds had been performed, Table 2 and Figure 1. Important calculated (practical) vibrational values had been found to be [3380 (3415) and 1653 (1670)], that corresponded to v(HO−) and v(-C=O), correspondingly, in the case of free **C1** ligand, while calculated (practical) vibrational values had been found to be [3522 (3475), 1679 (1607), and 598 (577)], [3495 (3473), 1642 (1612), and 609 (568)], and [3428 (3470), 1657 (1610), and 587 (572)] that corresponded to v(−OH), v(O=C−), and v(M-O), correspondingly, in the case of **C2**, **C3**, **C4** complexes, respectively.

3.2.3. Electronic Spectra and Magnetic Properties. Kindly refer to Figure 2a) and Table 3 for a comprehensive overview of the UV−vis spectra of **C1**, as well as its corresponding **C2**, **C4**, and **C3** counterparts in acetonitrile. The acquisition of these spectra involved measuring sample absorbance throughout a wavelength range that extended from 200 to 800 nm. It is worth mentioning that the observation of electronic spectrum bands at a wavelength of 345 nm may be ascribed to the transitions of **C1** from n → π*. The coordination of metal ions is responsible for the observed change in wavelength into

Table 3. UV-vis (Acetonitrile) and Effective Magnetic Moment Data of the Synthesized Compounds

	(C1)	(C2)	(C3)	(C4)
λ_{max}, nm	345	380, 475	440, 525	535, 630
μ_{eff} (B.M)	–	5.76	4.84	1.75
		d^5 high spin ($t_{2g}^3 e_g^2$)	d^7 high spin ($t_{2g}^5 e_g^2$)	d^9 ($e^4 t_2^5$)

longer values in this band where the wavelength shift was observed. In an effort to gain deeper insights into the composition of the metal complexes, an effective magnetic moment calculation method was employed, as outlined in Table 3. Moving on to **C2**, this compound exhibited electronic band with peak wavelengths of 380 and 475 nm. These bands are associated with the $^6A_{1g} \rightarrow T_{2g}(G)$ transition of the octahedral complex and ligand-to-metal charge transfer (LMCT), respectively. The Fe(III) center within the **C2** complex demonstrated a d^5 high spin ($t_{2g}^3 e_g^2$) configuration, evident based on the magnetic moment that was observed of 5.76 μ_B.[38] The **C3** complex displayed spectral bands at wavelengths of 525 and 440 nm, corresponding to the octahedral complexes $^4T_{1g}(F) \rightarrow {}^4A_{2g}(F)$ and $^4T_{1g}(F) \rightarrow {}^4T_{1g}(P)$, respectively.[39] The magnetic moment of 4.84 μ_B observed in **C3** in accordance with the magnetic moment that is expected to occur during the transition to the d^7 high spin ($t_{2g}^5 e_g^2$) configuration.[40−42] Lastly, the **C4** complex showcased two distinct bands at wavelengths of 535 and 630 nm, associated with the $^2B_{1g} \rightarrow {}^2E_{2g}$ and $^2B_{1g} \rightarrow {}^2A_{1g}$ configurations in the tetrahedral complex.[43] The presented data in Table 3 underscores that the **C4** complex displays a moment of magnetic attraction of 1.75 μ_B, aligning with a transition toward the d^9 ($e_g^4 t_{2g}5$) configuration.[44,45]

3.2.4. Molar Ratio of the C2, C4, and C3. The determination of the atomic composition of the metal compounds was facilitated through application of the molar ratio approach and Jobs' continuous variation methodology, as outlined in detail by previous studies.[46] In Figure 2b), the graphical representation vividly portrays the maximum absorbance levels observed across all metal complexes, reaching a peak at a ligand mole fraction of 0.66. This distinctive pattern strongly suggests the occurrence of a 1:2 (metal:ligand) formation within FeHNS, CoHNS, and CuHNS systems. This was shown by the data that were provided in Figure 2c), which demonstrated that the molar ratio strategy consistently produced results that were similar.

3.2.5. Thermal Behavior. 3.2.5.1. Thermal Behavior of C2, C4, and C3. The outcomes of our investigation into the thermal effects on metal complex compounds, encompassing the visual representations of structural features and water content, provide information in Figure (S.2) and are comprehensively tabulated in Table 4.[47]

In the initial phase of degradation, the **C2**, **C3**, and **C4** complexes experienced the loss of 3, 2, and 2 H_2O of hydration, respectively. Corresponding weight loss percent, calculated at 8.35 (8.73), 6.34 (6.14), and 6.21 (6.48), are meticulously detailed in Figure (S.2) and Table 4. Subsequently, during decomposition, the **C2** complex suffered the elimination of water and $C_{13}H_8ClN_2O_2$, while the **C3** complex witnessed the removal of $2H_2O$ and $C_{13}H_8N_2O_2$. Furthermore, the C4 complex underwent the expulsion of $C_{24}H_{12}N_2O_8$, with weight reduction percentages of 44.69 (44.86), 44.08 (44.33), and 82.26 (82.08) outlined in Figure (S.2) and Table 4.

Table 4. Thermal Decomposition of the C2, C4, and C3

	TG	DTG	mass loss (%)			residue (%)		
			found	calculated	assignment	found	calculated	assignment
C2	30−140	115	8.35	8.73	$3H_2O$	91.65	91.39	$[C_{24}H_{14}ClFeN_2O_9]$
	140−530	400	44.69	44.86	$H_2O + C_{13}H_8ClN_2O_2$	46.76	46.20	$[C_{11}H_2FeO_6]$
	530−800	585	37.07	37.18	$C_{11}H_2O_6$	9.29	9.02	Fe
C3	30−150	100	6.34	6.14	$2H_2O$	93.66	93.92	$[C_{24}H_{16}CoN_2O_{10}]$
	150−490	410	44.08	44.33	$2H_2O + C_{13}H_8N_2O_2$	49.48	49.59	$[C_{11}H_4CoO_6]$
	490−800	610	39.78	39.55	$C_{11}H_4O_6$	9.18	10.04	Co
C4	30−150	95	6.21	6.48	$2H_2O$	93.79	93.51	$C_{24}H_{12}CuN_2O_8$
	150−800	550	82.26	82.08	$C_{24}H_{12}N_2O_8$	11.53	11.43	Cu
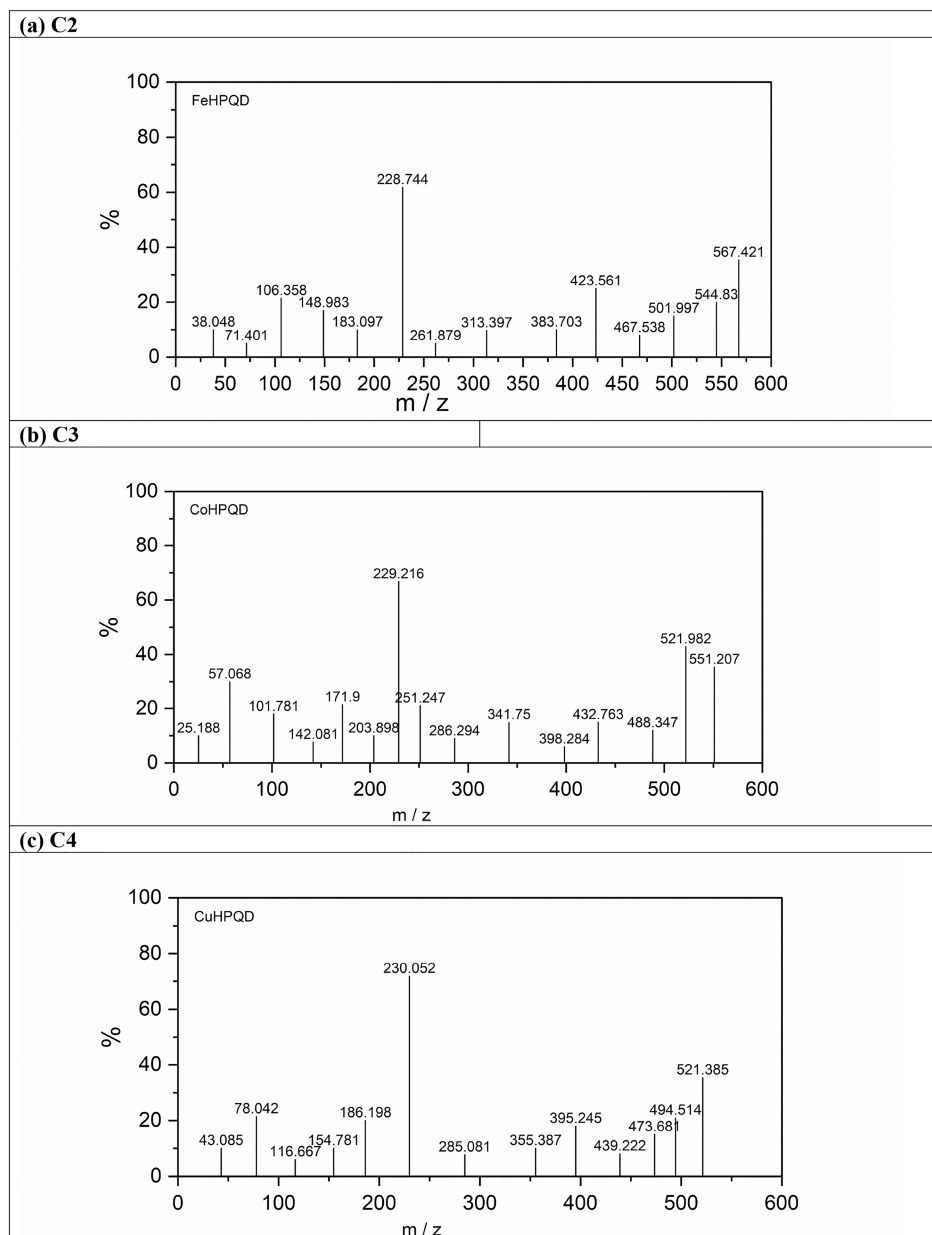
Figure 3. (a) Mass spectrum of **C2**, (b) mass spectrum of **C3**, and (c) mass spectrum of **C4**.

Notably, the disintegration of the **C4** complex undergoes a pause during the second phase, leading to the formation of metallic residue in the guise of copper metal. Conversely, the decomposition of **C2** and **C3** components occurs seamlessly. In the third decomposition step, both the $C_{11}H_2O_6$ derived from the **C2** complex and the $C_{11}H_4O_2$ derived that were derived from the C3 complex were removed, which led to the preservation of solely the metal parts as residue. Findings presented in Figure (S.2) and Table 4 illustrate a decrease in
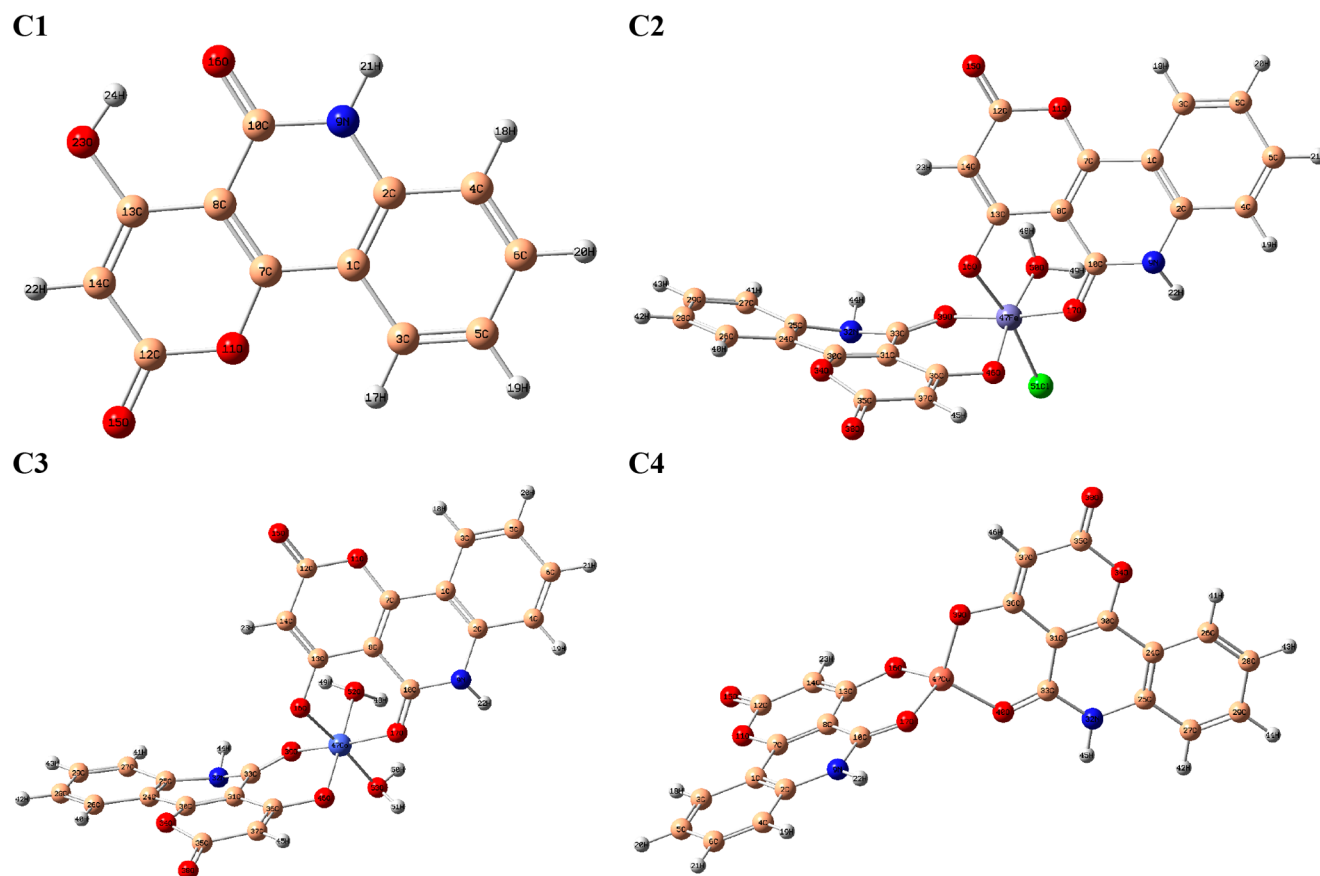
Figure 4. 3D, HOMO, LUMO, and MEP of the optimized structure of the target C1, C2, C3, and C4 compounds.

the percentage of additional weight by 37.07 (37.18) and 39.78 (39.55), respectively.

3.2.5.2. Kinetic and Thermodynamic Parameters Using Coats−Redfern Method. For each stage of the breakdown, the Coats-Redfern equation was used to evaluate the activation energy (E_a), entropy (ΔS), enthalpy (ΔH), and free energy change (ΔG).[48,49]

$$\ln\left[-\frac{\ln(1-\alpha)}{T^2}\right] = \ln\left[\frac{AR}{\beta\Delta E}\left(1-\frac{2RT}{E_a}\right)\right] - \frac{E}{RT}$$

where the rate of conversion of a decomposed solid is given by α, $(1\ 2RT/E) = 1$, ΔE is the activation energy, β is the linear heating rate, and A is the Arrhenius constant. The Coats-Redfern was plotted as $\ln\left[-\frac{\ln(1-\alpha)}{T^2}\right]$ against $\frac{1}{T}$, Figure (S.3). First-order kinetics had been confirmed by the Coats-Redfern plot displayed in Figure (S.3). The values of activation energy (E_a) and A were extracted from the slope and intercept, respectively. The thermodynamic parameters, entropy (ΔS), enthalpy (ΔH) and free energy change (ΔG), were evaluated using the following equations:[50]

$$\Delta S = 2.303RL\log\left(\frac{Ah}{k_BT}\right), \quad \Delta H = E_a - RT, \Delta G = \Delta H - T\Delta S$$

where h represents Planck's constant, Ts represents the temperature at which decomposition peaks, and K_B represents the Boltzmann constant. Table (S.1) summarizes these calculated values for the various parameters. From Table

(S1), the complexes have negative entropy (ΔS) and enthalpy (ΔH), while they have positive free energy change (ΔG). The thermodynamic parameters values for the examined complexes are quite similar. The results showed that the examined compounds degraded in a similar approach.

3.2.6. Mass Spectra. Elemental composition of compounds was validated through the utilization of mass spectrometry. Illustrated in Figure 3 are mass spectra of C2, C4, and C3 complexes. Mass spectra of these complexes had peaks that were associated with molecular ions (M^+) at m/z 567.421 $(M^+ - 3H_2O + 2)$, 551.207 $(M^+ - 2H_2O)$, and 521.385 $(M^+ - 2H_2O + 1)$, respectively. These discerned peaks aligned seamlessly with the expected values, affirming the accuracy of the proposed compositions. Additional peaks observed in the mass spectrum could potentially be attributed to minor constituents present in the C2, C4, and C3 complexes. Specifically, the peaks at 228.744 (for the Fe(III) complex), 229.216 (for the Co(II) complex), and 230.052 (for the Cu(II) complex) were attributed to the fragmentation of the organic ligand. The mass spectrometric results not only validated the practical values of carbon (C), hydrogen (H), and nitrogen (N) but also provided substantiating evidence for the proposed chemical formula.

3.3. DFT Calculations. Optimized structures of C2 and C3 revealed an octahedral configuration surrounding the metal center. Specifically, C2 was optimized as $[Fe(C1)_2(Cl)H_2O]$, while C4 adopted the representation $[Co(C1)_2(H_2O)_2]$, as depicted in Figure 4. The geometry of the metal center in C4 exhibited a four-coordinate structure, denoted as $[Cu(C1)_2]$.
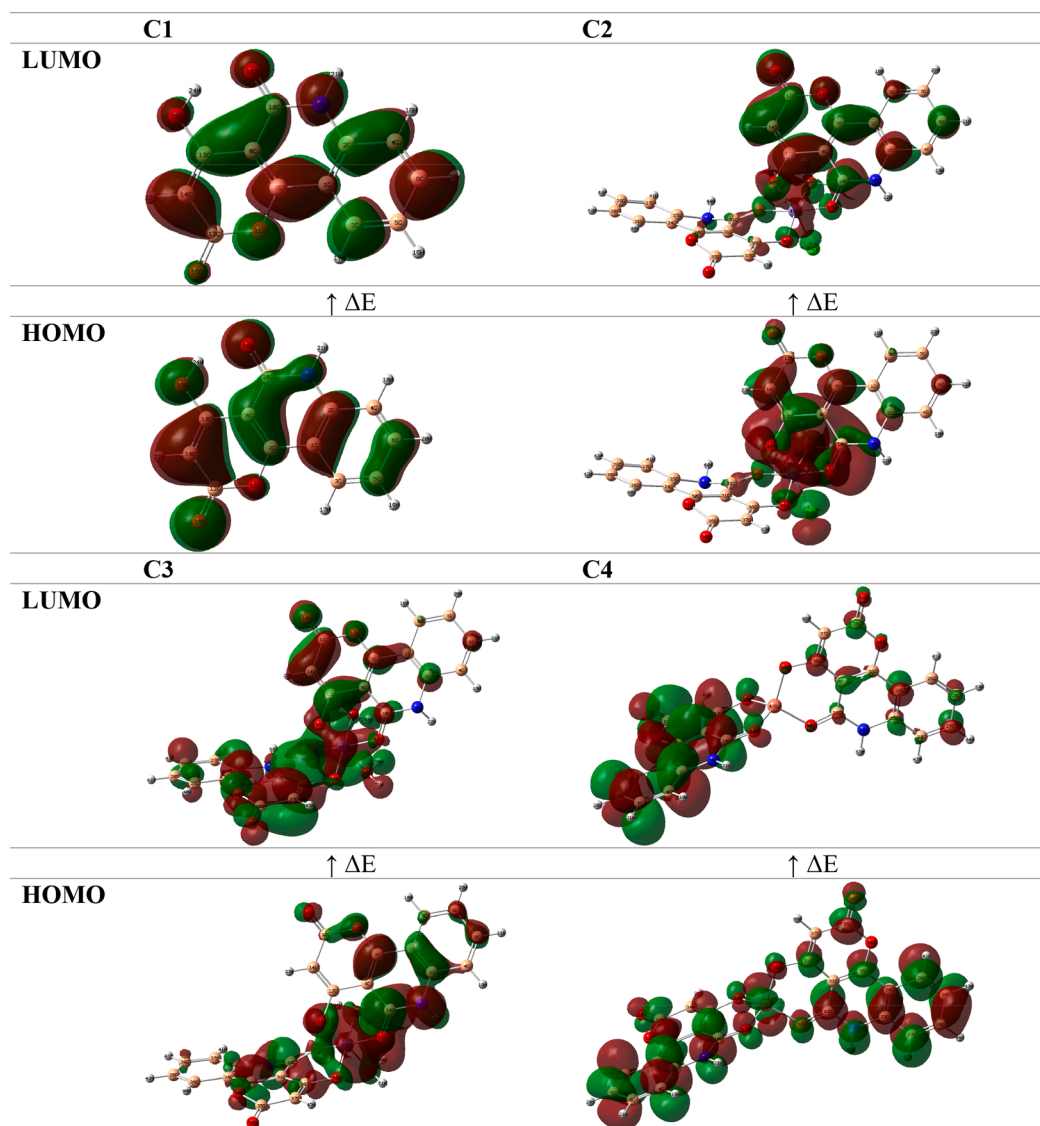
Figure 5. 3D, and HOMO−LUMO, in addition to MEP of the subject compounds.

Table 5. Calculated Parameters of the C1 and Its Corresponding C2, C3, and C4

	E_{HOMO} eV	E_{LUMO} eV	ΔE eV	IP eV	EA eV	χ eV	CP eV	η eV	σ eV^{-1}	ω eV	Nu eV
C1	−6.68	−2.51	4.17	6.68	2.51	4.59	−4.59	2.09	0.24	5.06	0.20
C2	−4.39	−3.08	1.32	4.39	3.08	3.73	−3.73	0.66	0.76	10.60	0.09
C3	−4.54	−2.67	1.88	4.54	2.67	3.60	−3.60	0.94	0.53	6.92	0.14
C4	−3.40	−1.89	1.51	3.40	1.89	2.65	−2.65	0.76	0.66	4.64	0.22

To confirm the tetrahedral geometry of the **C4** complex, the degree of distortion in the four-coordinate complex (T_4) was calculated using the formula $T_4 = (360 − (\alpha+\beta))/141$,[51] where α and β represent the two largest valence angles at the coordination center. The resulting degree of distortion, $T_4 = 0.645$ for the **C4** complex, indicated a distorted tetrahedral arrangement around the Cu(II) ion in the **C4** complex. This geometric analysis is visually presented in Figure 4.

The investigation was centered on the comprehensive examination of reactivity, chemical stability, and optical characteristics, employing frontier molecular orbitals (FMOs) known as the highest occupied molecular orbital (HOMO) and the lowest unoccupied molecular orbital (LUMO). As in Figure 5, spatial arrangement of the HOMO and the LUMO

across the components provides an illustration of the appearance of electron delocalization inside the molecules. The outcomes of computational analyses related to HOMO−LUMO gaps, electron affinities, ionization potentials, chemical potentials, electronegativities, chemical hardness, electrophilicity index, softness, and nucleophilicity are presented in Table 5. Understanding the HOMO and LUMO energies of a molecule holds significance in elucidating its biological activity, chemical reactivity, and hardness/softness dynamics.[52,53]

Scholars widely agree that electron donation predominantly occurs from the HOMO, characterized by its maximum electron density, while the LUMO, marked by deficiency of electrons, exhibits strong propensity to accept electrons from orbitals with greater levels of energy. The molecule's reactivity,
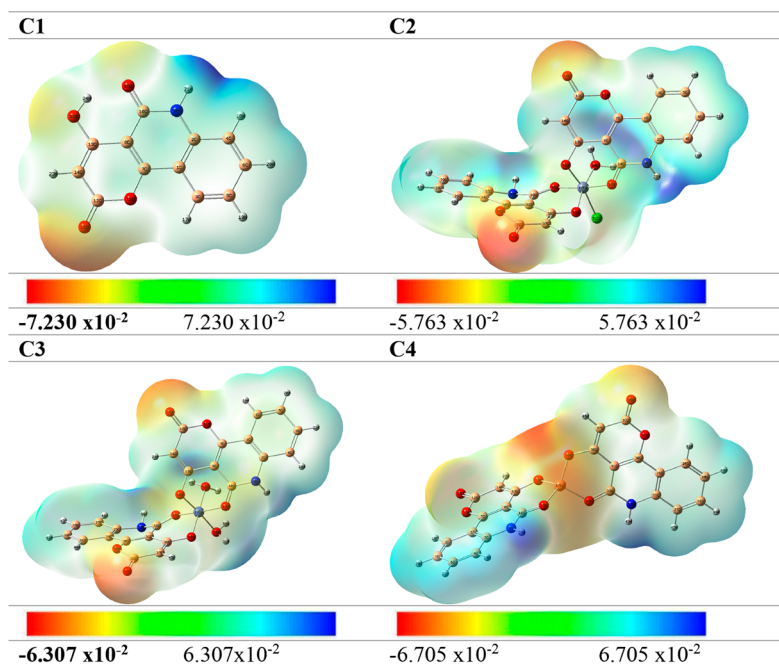
Figure 6. MEP of the subject compounds.

Table 6. Antimicrobial Activity of C1 and Its C2, C3, and C4 (Values = Average ± Standard Deviation)

		P. aeruginosa (-ve)	E. coli (-ve)	S. aureus (+ve)	B. cereus (+ve)	As. flavus	C. albicans
C1	IZ (mm)	9.20 ± 0.23	10.17 ± 0.19	9.19 ± 0.22	9.28 ± 0.30	8.27 ± 0.28	8.26 ± 0.24
	%	41.63 ± 0.85	52.97 ± 0.47	45.48 ± 0.66	40.01 ± 0.96	39.18 ± 1.01	35.60 ± 0.74
	MIC (μM)	225.63 ± 23.63	203.80 ± 5.77	225.63 ± 23.63	262.01 ± 10.00	225.63 ± 23.63	232.88 ± 5.77
C2	IZ (mm)	17.31 ± 0.30	19.21 ± 0.21	18.26 ± 0.24	17.21 ± 0.21	17.30 ± 0.30	16.22 ± 0.22
	%	78.34 ± 0.99	89.65 ± 0.26	90.40 ± 0.36	74.17 ± 0.27	81.99 ± 1.03	69.91 ± 0.33
	MIC (μM)	51.16 ± 7.64	51.16 ± 7.64	44.43 ± 13.92	51.16 ± 7.64	55.20 ± 19.42	51.16 ± 7.64
C3	IZ (mm)	20.23 ± 0.23	20.24 ± 0.24	19.23 ± 0.23	19.24 ± 0.26	18.20 ± 0.20	19.16 ± 0.18
	%	91.55 ± 0.61	94.98 ± 0.15	95.20 ± 0.20	82.93 ± 0.40	86.26 ± 0.54	82.59 ± 0.16
	MIC (μM)	58.21 ± 19.42	46.85 ± 13.92	35.49 ± 8.78	46.85 ± 13.92	53.95 ± 7.64	35.49 ± 8.78
C4	IZ (mm)	20.40 ± 0.40	19.13 ± 0.13	19.22 ± 0.22	18.30 ± 0.30	19.20 ± 0.20	18.22 ± 0.22
	%	92.31 ± 1.39	99.64 ± 0.36	95.15 ± 0.15	78.88 ± 0.61	91.00 ± 0.52	78.53 ± 0.27
	MIC (μM)	59.95 ± 5.77	47.97 ± 5.77	71.94 ± 10.00	53.96 ± 10.00	47.97 ± 5.77	53.96 ± 10.00

responsiveness to electrophilic and nucleophilic reactions, in addition to stability are contingent upon magnitudes of the HOMO and LUMO energies.[54] A reduction in the energy gap (ΔE) leads to an increase in the reactivity and docking probability of a molecule that describe the relatively greater activity of **C2** compared to **C4**, **C3**, and **C1**. The hard-soft-acid-base (HSAB) concept also influences the chemical reactivity of molecules.[53]

It is clear from this observation that there is a high probability that one molecule will create a chemical connection with another molecule. Hard acids tend to interact with other hard bases, while soft ones prefer establishing connections with soft ones. Biological molecules like cells, proteins, and macromolecules are inherently soft, suggesting that soft compounds have a higher propensity for forming bonds with their biological counterparts.[55] Table 5 provides a comparison examination, showing the notable enhancements in the softness and hardness of **C2**, **C4**, and **C3** compared to **C1**. The noticed rises in softness, consequent decreases in hardness, as presented in Table 5, positively impact biological activity.[56] A negative chemical potential indicates higher stability, and the expectation of distinguishing electrophilic

response is contingent upon the simultaneous occurrence of a significant electrophilicity index and a decreased chemical potential with respect to the substance in question.[57]

The exploration of the compounds' topological and structural properties in three-dimensions was conducted using the molecular electrostatic potential (MEP) diagram. This diagram serves as a metric for gauging the impact that nuclei or electrons have on the formation of the spatial arrangement.[58] In the MEP diagram, each value is represented by a different color gradient from blue to red, providing visual distinction. The MEP surface delineates regions of electrophilic and nucleophilic reactivity, appearing in blue and red, respectively.[59] Red dots on the surface signify areas with negative charge, indicating strong attraction toward electrophiles.[60] An increase in electrophilic interaction sites correlates with a decrease in the magnitude of the negative charge. The MEP diagram proposed for the components are illustrated in Figure 6, where areas adjacent to heteroatoms, particularly oxygen and nitrogen, exhibit elevated electron density, resulting in a negative charge denoted by the color red. These areas are more prone to electrophilic attack. The coordination complexes' water moiety and metal core display

Table 7. Antioxidant Data of the Free C1 and Its C2, C3, and C4

	C1	C2	C3	C4	ascorbic acid
IC$_{50}$ (μM)	87.5 ± 1.04	60.7 ± 0.87	55.4 ± 0.94	76.2 ± 0.88	36.1 ± 0.76
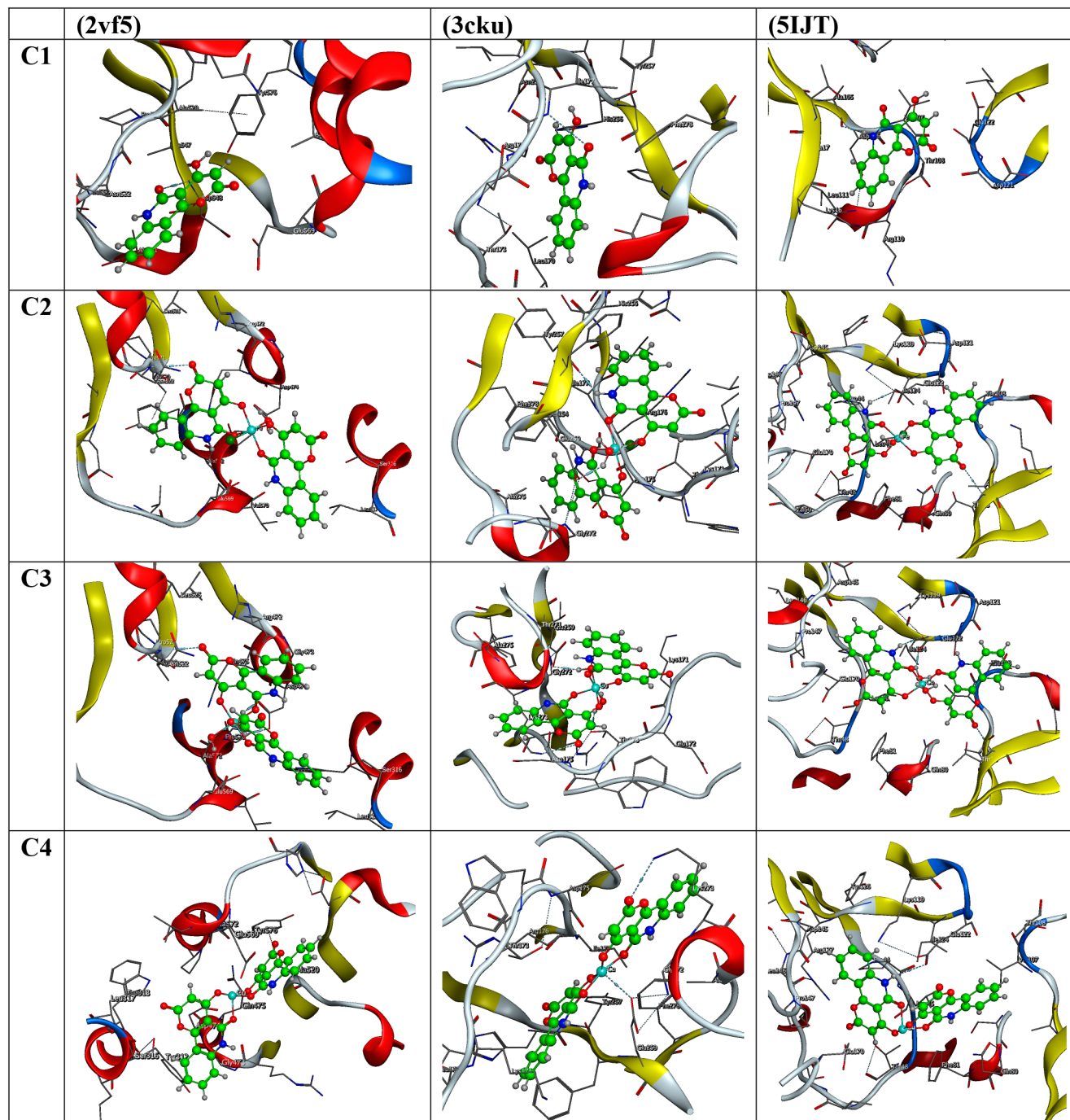
Figure 7. 3D interactions of the ligand-protein complex.

positively charged regions, represented in blue in Figure 6. These positively charged regions have the potential to function as hydrogen bond donors in intermolecular interactions involving proteins. The visual depiction of MEP aids in understanding the spatial distribution of charge, offering insights into potential reactivity and interaction patterns within the molecular structure.

3.4. Biological Effectiveness. *3.4.1. In Vitro Antimicrobial.* The biological studies were done in DMSO as solvent. It is a common solvent used in biological studies because it can dissolve both polar and nonpolar compounds,[61] and also, herein, it provides good solubility of the studied components. First, the stability of current components in the used solvent was checked by observing the absorbance change of the current compounds at various time intervals. It was observed

that the current compounds have good stability in the used solvent even after long time periods, Figure (S.4).

The antifungal and antibacterial activities of the compounds were assessed against *Candida albicans*, *Aspergillus flavus*, *Trichophyton rubrum*, *Escherichia coli*, *Staphylococcus aureus*, and *Pseudomonas aeruginosa*. The measurement and documentation of the zone of inhibition (ZI) produced via each component were conducted and recorded in Table 6. Notably, **C2**, **C4**, and **C3** exhibited heightened biological effectiveness and larger zones of inhibition in comparison to the unbound ligand. Improved reactivity of **C2**, **C4**, and **C3** can be elucidated through the application of chelation theory.[62] The polarity of metal ions may be successfully reduced by the process of chelation, which involves the transfer of their positive charge to electron-donating groups.[63] This process results in the distribution of electrons throughout the entire structure, enhancing the compound's affinity for lipids and enabling it to traverse the lipid bilayer of cellular membranes.

Through this mechanism, the chemical compound gains the ability to bind to bacterial active sites, disrupting their metabolic pathways and respiratory functions. This interference impedes protein synthesis and microorganism proliferation, ultimately leading to their demise. Evaluation of the compounds' zone of inhibition (ZI) width in contrast to the standard Ciprofloxacin, which revealed a substantial increase in % activity index, as reported in the experimental section 2.4.1. The inhibitory efficacy against *E. coli* showed varying values, with free **C1** displaying a percent of 52.97%, **C2** at 99.64%, **C3** at 94.98%, and **C4** at 99.67%. The minimum inhibitory concentration (MIC), in μM, was strongminded through a series of dilution processes. It was observed that the complexes exhibited a greater degree of inhibition versus all of the strains that were tested in comparison to the free ligand, as indicated in the data presented in Table 6.

3.4.2. Antioxidant Activity. A wide variety of naturally occurring and synthetically manufactured chemicals have the capacity to inhibit or delay the destructive effects of free radicals on cellular structures; these compounds are referred to together as antioxidants.[64,65] Regular biological activities result in the production of free radicals, also known as reactive oxygen species (ROS). The significance of reactive oxygen species (ROS) in a wide variety of cell signaling pathways is essential. However, numerous adverse consequences, including those on the nervous system, the development of cancer, metabolic dysfunctions, the beginning of inflammation, and cellular senescence, may come from an excess or uncontrolled formation of reactive oxygen species (ROS).[64,65] Through metabolic and signaling modifications, the human body possesses various antioxidant defense systems that efficiently regulate ROS production. Damage to cellular structures and even death may occur if antioxidant defense systems are unable to reduce levels of reactive oxygen species (ROS). Since metal complexes show promise for the creation of novel pharmacological treatments, it is important to study their antioxidant properties.[66] The antioxidant performance of the metal complex compounds were evaluated in this study via the DPPH approach.

The *in vitro* antioxidant activity of the free ligand **C1** and its complex compounds **C2**, **C4**, and **C3** was assessed using the DPPH method. The DPPH (2,2-diphenyl-1-picrylhydrazyl) radical, a chemically stable free radical with a dark purple color, was employed to measure the compounds' efficacy by determining the reduction of the purple DPPH solution. The

data, presented in Table 7, indicated that the metal complex compounds exhibited stronger antioxidant effectiveness compared to the free ligand. Vitamin C served as the reference substance for additional comparisons. As said by the data in Table 7, both the free ligand **C1** and its complexes **C2**, **C4**, and **C3** displayed antioxidant properties comparable to those of ascorbic acid.

The IC_{50} value was found to be 55.4 ± 0.94 μM for the **C3** complex, 60.7 ± 0.87 μM for the **C2** complex, and 76.2 ± 0.88 μM for the **C4** complex. Substances with higher free radical activity have lower IC_{50} values. Table 7 demonstrates that the **C2**, **C4**, and **C3** have good antioxidant properties than those of the free **C1** ($IC_{50} = 87.5 \pm 1.04$ μM).

3.5. Molecular Docking. The investigation encompassed the execution of molecular docking targeting three proteins: 2vf5 from *Escherichia coli*, 3cku from *Aspergillus flavus*, and 5IJT. The docking postures and compound-protein interactions in 2D and 3D are depicted in Figure (S.5) and Figure 7, respectively. In-depth information about the bonding energy and bond interaction energy for each and every compound-protein association are presented in Table (S.2).

Employing molecular docking techniques, an analytical exploration was undertaken to elucidate the interaction patterns of various chemical compounds with the respective receptors.[23,67] Table (S.2) compiles observed distances in diverse bonding types, encompassing hydrogen bonds. Variances in binding affinities were noted across different receptors. For complexes 2vf5 and 3cku, the order of binding affinity is **C4** > **C2** > **C3** > **C1**, whereas for complex 5IJT, the order is **C3** > **C2** > **C4** > **C1**.

The results signify those compounds with stronger interactions, such as **C4** (for 2vf5 and 3cku) and **C2** (for 5IJT), had high binding affinity in comparison to the free **C1**. These molecules engage in various hydrogen, ionic, and pi-H interactions within receptor.[68] The kinds of bonds and the distances that correspond to them that were detected in the interactions that took place inside the 2vf5, 3cku, and 5IJT receptors are comprehensively described in Table (S.2).

According to the results, the C4 complex had the highest level of binding affinity against the 2vf5 receptor, as described by docking score (S) of −6.70 kcal/mol, which was the lowest among all tested complexes. Four ionic interactions were observed between the amino acid residues SER316 and N49, as well as S53, at distances of 2.91 and 3.07 Å, respectively. Four ionic interactions were created at certain distances: 3.48, 3.81, 4.00, and 2.94 nm. These interactions occurred between the atoms N9-GLU569, O17-GLU568, N32-ASP474, and O40-ASP474, respectively. Aside from that, the **C4** complex showed the formation of two pi-H interactions at positions 4.81 and 4.19, involving the 6-ring-GLY473 and 6-ring-ASP474 residues. The calculated docking score (S) for the unbound **C1** ligand was determined to be −4.78 kcal/mol, indicating a somewhat weaker affinity for the 2vf5 receptor in comparison to the other ligand−receptor complexes. Between O16-ASP 548 and 6-ring-ASN522, a single hydrogen acceptor and a single pi-hydrogen interaction were observed at positions 3.02 and 4.03, respectively.

The **C4** complex exhibited the highest affinity aganist 3cku receptor, as publicized via a docking score (S) of −6.99 kcal/ mol. The formation of a 2.84 H-acceptor bond between O38 and LYS273 was observed. Additionally, the occurrence of one metal, two ionic, and two pi-H interactions was seen at distances of 2.66, 2.94, 3.20, 3.84, and 4.56 Å between the

CU47-GLU259, O17-GLU259, O40-GLU259, 6-ring-ASP175, and 6-ring-ALA275 entities. The obtained docking score (S) of −5.48 kcal/mol for the unbound **C1** ligand indicates a lower affinity toward the 3cku receptor in comparison to the other complexes. A single H-acceptor bond at a distance of 3.24 and a single pi-H bond at a distance of 3.82 were established between the oxygen atom (O16) of isoleucine residue 177 (ILE177) and the arginine residue 176 (ARG176) located in the six-membered ring.

The **C3** complex exhibited a docking score (S) of −7.95 kcal/mol while interacting with the 5IJT receptor, indicating a strong binding affinity between the two entities. Hydrogen bonds were seen to form at the coordinates 3.19, 2.50, and 3.25, involving the interactions with N9-GLU122, O52-GLU122, and O38-THR18, respectively. Furthermore, a pi-cation contact was established between the 6-ring and LYS119 at a distance of 4.77. Additionally, four ionic connections were formed involving N9-GLU122, O17-GLU122, O39-GLU122, and O52-GLU122 at distances of 3.49, 2.86, 3.15, and 2.50, respectively. The calculated docking score (S) for the unbound **C1** ligand was determined to be −5.85 kcal/mol, indicating a somewhat weaker binding affinity to the 5IJT receptor in comparison to the other ligand−receptor complexes. At the coordinates 2.94 and 3.50, a singular hydrogen-donor bond was formed between the nitrogen atom at position 9 and the alanine residue at position 105.

3.6. Molecular Docking and *In Vitro* Biological Activities Correlation. While *in vitro* tests demonstrated that metal complexes exhibit superior antibacterial, antifungal, and antioxidant efficacy in comparasion with the free ligand, a correlation between *in vitro* activity and *in silico* molecular docking studying is evident, as indicated in Table (S.2) and Section 3.5. The findings suggest that metal complexes surpass the corresponding free ligand in terms of activity. The docking results revealed a consistent order of binding affinity, with **C4** > **C2** > **C3** > **C1** against 2vf5 and 3cku, and **C3** > **C2** > **C4** > **C1** against 5IJT. This order aligns with the experimental data, reinforcing the robustness of the observed positive association between experimental and computational results.

4. CONCLUSION

Three newly synthesized compounds, denoted as **C2**, **C3**, and **C4**, underwent comprehensive characterization of their physicochemical and spectroscopic attributes. Our investigation revealed that the **C1** ligand exhibited monobasic bidentate OO ligand behavior when complexed with Fe(III), Co(II), and Cu(II) at a molar ratio of 1:2. Analyzing the data from both analytical and spectroscopic perspectives led to the hypothesis that the **C2** and **C3** complexes adopted octahedral geometries, while the **C4** complex adopted tetrahedral geometry. Subsequent to the theoretical optimization of the molecular structures of these metal complexes, an exploration of calculated chemical parameters was undertaken. In parallel, *in vitro* experiments were conducted to assess the antioxidant, antimicrobial, and antibacterial properties of the ligand and its corresponding complexes. The outcomes of the study revealed that the complexes exhibited greater activity as antifungal, antibacterial, and antioxidant candidates in comparasion with the free ligand. Furthermore, molecular docking analyses were performed to scrutinize the binding affinities of the compounds against three specific target proteins: 2vf5 from *Escherichia coli*, 3cku from *Aspergillus flavus*, and 5IJT (crystal structure of human peroxiredoxin 2 oxidised). Among the compounds, **C4**

and **C3** exhibited the most notable antibacterial and antioxidant activities, respectively.

■ ASSOCIATED CONTENT

Data Availability Statement

The data sets supporting this article have been uploaded as part of the electronic Supporting Information.

Ⓢ Supporting Information

The Supporting Information is available free of charge at https://pubs.acs.org/doi/10.1021/acsomega.3c06274.

(S.1.) Synthesis of the 4-hydroxy-2H-pyrano[3,2-*c*]-quinoline-2,5(6H)-dione (1)) ligand; (S.2.) characterization; (S.3.) antioxidant activity; (S.4.) characterization of the (1) ligand; Figure (S1): (a), (b) ^{1}H NMR and (c) ^{13}C NMR of the 4-hydroxy-2H-pyrano-[3,2-*c*]quinoline-2,5(6H)-dione ligand; Figure (S.2) (a) thermal decomposition of (2), (b) thermal decomposition of (3), and (c) thermal decomposition of (4); Figure (S.3) Coats-Redfern plot and its linear fit of the studied complexes; Figure (S.4) stability of the current compounds in DMSO as absorbance change at various time intervals; Figure (S.5) 2D interactions of the ligand-protein complex; Table (S.1) the activation parameters of decomposition steps as derived from Coats-Redfern plots of the studied complexes; and Table (S.2) molecular docking results (PDF)

■ AUTHOR INFORMATION

Corresponding Authors

Hany M. Abd El-Lateef − *Department of Chemistry, College of Science, King Faisal University, Al-Ahsa 31982, Saudi Arabia; Department of Chemistry, Faculty of Science, Sohag University, Sohag 82524, Egypt;* ⓞ orcid.org/0000-0002-6610-393X; Email: hmahmed@kfu.edu.sa, hany_shubra@science.sohag.edu.eg

Aly Abdou − *Department of Chemistry, Faculty of Science, Sohag University, Sohag 82524, Egypt;* ⓞ orcid.org/0000-0002-5979-2650; Email: aly_abdou@science.sohag.edu.eg, aly_abdou@yahoo.com

Authors

Mai M. Khalaf − *Department of Chemistry, College of Science, King Faisal University, Al-Ahsa 31982, Saudi Arabia; Department of Chemistry, Faculty of Science, Sohag University, Sohag 82524, Egypt*

Mohamed Gouda − *Department of Chemistry, College of Science, King Faisal University, Al-Ahsa 31982, Saudi Arabia*

Antar A. Abdelhamid − *Department of Chemistry, Faculty of Science, Sohag University, Sohag 82524, Egypt; Department of Chemistry, Faculty of Science, Al-Baha University, Al-Baha 65635, Saudi Arabia*

Amer A. Amer − *Department of Chemistry, Faculty of Science, Sohag University, Sohag 82524, Egypt;* ⓞ orcid.org/0000-0001-7112-9918

Complete contact information is available at:
https://pubs.acs.org/10.1021/acsomega.3c06274

Author Contributions

M.M.K.: Investigation, methodology, resources, formal analysis, data curation, funding acquisition, writing-original draft, and writing-review and editing. H.M.A.E.-L.: Investigation, funding acquisition, writing-original draft, and writing-review

and editing. M.G.: Investigation, funding acquisition, writing-original draft, and writing-review and editing. A.A.A.: Investigation, supervision, methodology, resources, formal analysis, data curation, funding acquisition, writing-original draft, and writing-review and editing. A.A.A.: Investigation, supervision, methodology, resources, formal analysis, data curation, funding acquisition, writing-original draft, and writing-review and editing. A.A.: Investigation, supervision, methodology, resources, formal analysis, data curation, funding acquisition, writing-original draft, and writing-review and editing. All authors have read and agreed to the published version of the manuscript.

Notes

This manuscript does not include any experiments on humans or animals.

The authors declare no competing financial interest.

■ REFERENCES

(1) Rajesh, Y. B. Quinoline heterocycles: synthesis and bioactivity. In *Heterocycles-Synthesis and Biological Activities*; IntechOpen, 2018.

(2) Thurner, F.; Alatraktchi, F. A. a. Recent Trends in Biosensors for Quinolone Detection: A Comprehensive Review. *Chemosensors* 2023, *11* (9), 493.

(3) Măciucă, A.-M.; Munteanu, A.-C.; Uivarosi, V. Quinolone complexes with lanthanide ions: An insight into their analytical applications and biological activity. *Molecules* 2020, *25* (6), 1347.

(4) Kaur, T.; Bhandari, D. D. Annotated Review on Various Biological Activities of Quinoline Molecule. *Biointerface Res. Appl. Chem.* 2023, *13* (4), 355.

(5) Senerovic, L.; Opsenica, D.; Moric, I.; Aleksic, I.; Spasić, M.; Vasiljevic, B. Quinolines and quinolones as antibacterial, antifungal, anti-virulence, antiviral and anti-parasitic agents. *Adv. Exp. Med. Biol.* 2020, *1282*, 37−69.

(6) Kappe, T.; Aigner, R.; Hohengassner, P.; Stadlbauer, W. Syntheses of 3-Acyl-4-hydroxy-2 (1H) quinolones. *Journal für Praktische Chemie/Chemiker-Zeitung* 1994, *336* (7), 596−601.

(7) Abdou, M. M. Chemistry of 4-hydroxy-2 (1H)-quinolone. Part 2. As synthons in heterocyclic synthesis. *Arabian Journal of Chemistry* 2018, *11* (7), 1061−1071.

(8) Abdou, M. M. Chemistry of 4-Hydroxy-2 (1H)-quinolone. Part 1: Synthesis and reactions. *Arabian Journal of Chemistry* 2017, *10*, S3324−S3337.

(9) Fayed, T. A.; Gaber, M.; Abu El-Reash, G. M.; El-Gamil, M. M. Structural, DFT/B3LYP and molecular docking studies of binuclear thiosemicarbazide Copper (II) complexes and their biological investigations. *Appl. Organomet. Chem.* 2020, *34* (9), No. e5800.

(10) Anu; Srivastava, A.; Khan, M. S. Density functional theory calculations for electronic, optoelectronic and thermodynamic properties of dibenzothiophene metal complexes. *Mater. Res. Express* 2020, *7* (1), No. 016311.

(11) Dhonnar, S. L.; Sadgir, N. V.; Adole, V. A.; Jagdale, B. S. Molecular structure, FT-IR spectra, MEP and HOMO-LUMO investigation of 2-(4-fluorophenyl)-5-phenyl-1, 3, 4-oxadiazole using DFT theory calculations. *Advanced Journal of Chemistry-Section A* 2021, *4* (3), 220−230.

(12) AYTEMIZ, F.; BEYTUR, M.; YUKSEK, H. Experimental and Gaussian calculations of 3-Ethyl-4-(2-benzenesulfonyloxy)-benzylideneamino-4, 5-dihydro-1H-1, 2, 4-triazol-5-one. *Eurasia Proceedings of Science Technology Engineering and Mathematics* 2022, *20*, 103−111.

(13) Abdou, A.; Omran, O. A.; Al-Fahemi, J. H.; Jassas, R. S.; Al-Rooqi, M. M.; Hussein, E. M.; Moussa, Z.; Ahmed, S. A. Lower rim thiacalixarenes derivatives incorporating multiple coordinating carbonyl groups: Synthesis, characterization, ion-responsive ability and DFT computational analysis. *J. Mol. Struct.* 2023, *1293*, No. 136264.

(14) Abd El-Lateef, H. M.; Khalaf, M. M.; Amer, A. A.; Kandeel, M.; Abdelhamid, A. A.; Abdou, A. Synthesis, Characterization, Antimicrobial, Density Functional Theory, and Molecular Docking Studies of Novel Mn (II), Fe (III), and Cr (III) Complexes Incorporating 4-(2-Hydroxyphenyl azo)-1-naphthol (Az). *ACS omega* 2023, *8* (29), 25877−25891.

(15) El-Remaily, M. A. E. A. A. A.; Elhady, O.; Abdou, A.; Alhashmialameer, D.; Eskander, T. N. A.; Abu-Dief, A. M. Development of new 2-(Benzothiazol-2-ylimino)-2,3-dihydro-1H-imidazol-4-ol complexes as a robust catalysts for synthesis of thiazole 6-carbonitrile derivatives supported by DFT studies. *J. Mol. Struct.* 2023, *1292*, No. 136188.

(16) Arafath, M. A.; Adam, F.; Ahamed, M. B. K.; Karim, M. R.; Uddin, M. N.; Yamin, B. M.; Abdou, A. Ni (II), Pd (II) and Pt (II) complexes with SNO-group thiosemicarbazone and DMSO: Synthesis, characterization, DFT, molecular docking and cytotoxicity. *J. Mol. Struct.* 2023, *1278*, No. 134887.

(17) Balouiri, M.; Sadiki, M.; Ibnsouda, S. K. Methods for in vitro evaluating antimicrobial activity: A review. *Journal of pharmaceutical analysis* 2016, *6* (2), 71−79.

(18) Hossain, M.; Khushy, K.; Latif, M.; Hossen, M. F.; Asraf, M. A.; Kudrat-E-Zahan, M.; Abdou, A. Co (II), Ni (II), and Cu (II) Complexes Containing Isatin-Based Schiff Base Ligand: Synthesis, Physicochemical Characterization, DFT Calculations, Antibacterial Activity, and Molecular Docking Analysis. *Russ. J. Gen. Chem.* 2022, *92* (12), 2723−2733.

(19) Abd El-Lateef, H. M.; Khalaf, M. M.; El-Taib Heakal, F.; Abdou, A. Fe(III), Ni(II), and Cu(II)-moxifloxacin-tri-substituted imidazole mixed ligand complexes: Synthesis, structural, DFT, biological, and protein-binding analysis. *Inorg. Chem. Commun.* 2023, *158*, No. 111486.

(20) Struga, M.; Roszkowski, P.; Bielenica, A.; Otto-Slusarczyk, D.; Stepien, K.; Stefanska, J.; Zabost, A.; Augustynowicz-Kopec, E.; Kolinski, M.ł; Kmiecik, S.; Myslovska, A.; Wrzosek, M.łg. N-Acylated Ciprofloxacin Derivatives: Synthesis and In Vitro Biological Evaluation as Antibacterial and Anticancer Agents. *ACS omega* 2023, *8*, 18663.

(21) Çakmak, R.; Ay, B.; Çınar, E.; Başaran, E.; Akkoç, S.; Boğa, M.; Taş, E. Synthesis, spectroscopic, thermal analysis and in vitro cytotoxicity, anticholinesterase and antioxidant activities of new Co (II), Ni (II), Cu (II), Zn (II), and Ru (III) complexes of pyrazolone-based Schiff base ligand. *J. Mol. Struct.* 2023, *1292*, No. 136225.

(22) Abu-Dief, A. M.; El-Khatib, R. M.; El-Dabea, T.; Abdou, A.; Aljohani, F. S.; Al-Farraj, E. S.; Barnawi, I. O.; Remaily, M. A. E. A. A. Fabrication, structural elucidation of some new metal chelates based on N-(1H-Benzoimidazol-2-yl)-guanidine ligand: DNA interaction, pharmaceutical studies and molecular docking approach. *J. Mol. Liq.* 2023, *386*, No. 122353.

(23) Najar, A. M.; Eswayah, A.; Moftah, M. B.; Omar, M.K. R.; Bobtaina, E.; Najwa, M.; Elhisadi, T. A.; Tahani, A.; Tawati, S. M.; Khalifa, A. M. M.; Abdou, A.; Emhamed DowAltome, A. Rigidity and Flexibility of Pyrazole, s-Triazole, and v-Triazole Derivative of Chloroquine as Potential Therapeutic against COVID-19. *Journal of Medicinal and Chemical Sciences* 2023, *6* (9), 2056−2084.

(24) Al-Gaber, M. A. I.; Abd El-Lateef, H. M.; Khalaf, M. M.; Shaaban, S.; Shawky, M.; Mohamed, G. G.; Abdou, A.; Gouda, M.; Abu-Dief, A. M. Design, Synthesis, Spectroscopic Inspection, DFT and Molecular Docking Study of Metal Chelates Incorporating Azo Dye Ligand for Biological Evaluation. *Materials* 2023, *16* (3), 897.

(25) Abd El-Lateef, H. M.; Khalaf, M. M.; Kandeel, M.; Amer, A. A.; Abdelhamid, A. A.; Abdou, A. Designing, characterization, biological, DFT, and molecular docking analysis for new FeAZD, NiAZD, and CuAZD complexes incorporating 1-(2-hydroxyphenylazo)− 2-naphthol (H2AZD). *Comput. Biol. Chem.* 2023, *105*, No. 107908.

(26) Murugan, T.; Venkatesh, R.; Geetha, K.; Abdou, A. Synthesis, Spectral Investigation, DFT, Antibacterial, Antifungal and Molecular Docking Studies of Ni (II), Zn (II), Cd (II) Complexes of Tetradentate Schiff-Base Ligand. *Asian J. Chem.* **2023**, *35*, 1509−1517.

(27) El-Saghier, A. M.; Enaili, S. S.; Kadry, A. M.; Abdou, A.; Gad, M. A. Green synthesis, biological and molecular docking of some novel sulfonamide thiadiazole derivatives as potential insecticidal against Spodoptera littoralis. *Sci. Rep.* **2023**, *13* (1), 19142.

(28) Shah, R.; Alharbi, A.; Hameed, A. M.; Saad, F.; Zaky, R.; Khedr, A. M.; El-Metwaly, N. Synthesis and structural elucidation for new Schiff base complexes; conductance, conformational, MOE-docking and biological studies. *Journal of Inorganic and Organometallic Polymers and Materials* **2020**, *30*, 3595−3607.

(29) Ogunwa, T. Phyto-constituents obtained from Tanzanian medicinal plants display a high potential to inhibit Glucosamine-6-phosphate synthase as an antimicrobial target. *Journal of Biological Engineering Research and Review* **2017**, *4* (1), 20−33.

(30) El-Metwaly, N. M.; El-Ghalban, M. G. Hartree-Fock, molecular docking, spectral, kinetic and antitumor considerations for cobalt, nickel, palladium and platinum (II)-bis carbothiohydrazide complexes. *J. Mol. Liq.* **2016**, *220*, 265−276.

(31) Chen, X.; Zhao, Y.; Luo, W.; Chen, S.; Lin, F.; Zhang, X.; Fan, S.; Shen, X.; Wang, Y.; Liang, G. Celastrol induces ROS-mediated apoptosis via directly targeting peroxiredoxin-2 in gastric cancer cells. *Theranostics* **2020**, *10* (22), 10290.

(32) Elkanzi, N. A.; Hrichi, H.; Salah, H.; Albqmi, M.; Ali, A. M.; Abdou, A. Synthesis, physicochemical properties, biological, molecular docking and DFT investigation of Fe (III), Co (II), Ni (II), Cu (II) and Zn (II) complexes of the 4-[(5-oxo-4, 5-dihydro-1, 3-thiazol-2-yl) hydrazono] methyl} phenyl 4-methylbenzenesulfonate Schiff-base ligand. *Polyhedron* **2023**, *230*, No. 116219.

(33) Hashem, H. E.; Nath, A.; Kumer, A. Synthesis, molecular docking, molecular dynamic, quantum calculation, and antibacterial activity of new Schiff base-metal complexes. *J. Mol. Struct.* **2022**, *1250*, No. 131915.

(34) Latif, M.; Ahmed, T.; Hossain, M. S.; Chaki, B.; Abdou, A.; Kudrat-E-Zahan, M. Synthesis, Spectroscopic Characterization, DFT Calculations, Antibacterial Activity, and Molecular Docking Analysis of Ni (II), Zn (II), Sb (III), and U (VI) Metal Complexes Derived from a Nitrogen-Sulfur Schiff Base. *Russian Journal of General Chemistry* **2023**, *93* (2), 389−397.

(35) Shaaban, S.; Abdou, A.; Alhamzani, A. G.; Abou-Krisha, M. M.; Al-Qudah, M. A.; Alaasar, M.; Youssef, I.; Yousef, T. A. Synthesis and in silico investigation of organoselenium-clubbed schiff bases as potential Mpro inhibitors for the SARS-CoV-2 replication. *Life* **2023**, *13* (4), 912.

(36) Samy, F.; Shebl, M. Synthesis, spectroscopic, biological, and theoretical studies of new complexes from (E)-3-(2-(5, 6-diphenyl-1, 2, 4-triazin-3-yl) hydrazono) butan-2-one oxime. *Appl. Organomet. Chem.* **2020**, *34* (4), No. e5502.

(37) Khalaf, M. M.; El-Lateef, H. M. A.; Gouda, M.; Amer, A. A.; Abdelhamid, A. A.; Taleb, M. F. A.; Alfarsi, A.; Ibrahim, T. M. A.; El-Shamy, H.; Abdou, A. Synthesis, characterization, DFT, biological activity evaluation, and molecular docking analysis of new 8-[(2-hydroxynaphthalen-1-yl)diazenyl]naphthalene-1,3-disulfonic acid based complexes. *J. Mol. Struct.* **2024**, *1300*, No. 137175.

(38) Refat, M. S.; Altalhi, T.; Bakare, S. B.; Al-Hazmi, G. H.; Alam, K. New Cr (III), Mn (II), Fe (III), Co (II), Ni (II), Zn (II), Cd (II), and Hg (II) gibberellate complexes: synthesis, structure, and inhibitory activity against COVID-19 protease. *Russian Journal of General Chemistry* **2021**, *91* (5), 890−896.

(39) Al-Amery, M. H.; Al-Sahlanee, T. Q. M. Synthesis, characterization, antioxidant and anticancer human studies of new metal ion complexes of poly schiff base derived from 4-aminoacetophenone with 4-chloroaniline and salicylaldehyde. *Res. J. Chem. Environ* **2019**, *23*, 200−227.

(40) El-Shafiy, H. F.; Saif, M.; Mashaly, M. M.; Halim, S. A.; Eid, M. F.; Nabeel, A.; Fouad, R. New nano-complexes of Zn (II), Cu (II), Ni

(II) and Co (II) ions; spectroscopy, thermal, structural analysis, DFT calculations and antimicrobial activity application. *J. Mol. Struct.* **2017**, *1147*, 452−461.

(41) Altun, Ö.; Şuözer, M. Synthesis, spectral analysis, stability constants, antioxidant and biological activities of Co (II), Ni (II) and Cu (II) mixed ligand complexes of nicotinamide, theophylline and thiocyanate. *J. Mol. Struct.* **2017**, *1149*, 307−314.

(42) Drzewiecka-Antonik, A.; Ferenc, W.; Wolska, A.; Klepka, M. T.; Cristóvão, B.; Sarzyński, J.; Rejmak, P.; Osypiuk, D. The Co (II), Ni (II) and Cu (II) complexes with herbicide 2, 4-dichlorophenoxyacetic acid−Synthesis and structural studies. *Chem. Phys. Lett.* **2017**, *667*, 192−198.

(43) Devi, J.; Yadav, M.; Jindal, D.; Kumar, D.; Poornachandra, Y. Synthesis, spectroscopic characterization, biological screening and in vitro cytotoxic studies of 4-methyl-3-thiosemicarbazone derived Schiff bases and their Co (II), Ni (II), Cu (II) and Zn (II) complexes. *Appl. Organomet. Chem.* **2019**, *33* (10), No. e5154.

(44) Alamri, M. A.; Al-Jahdali, M.; Al-Radadi, N. S.; Hussien, M. A. Characterization, theoretical investigation, and biological applications of Mn (II), Co (II), Ni (II), Cu (II), and Zn (II) complexes of a triazene ligand containing a benzothiazole ring. *Appl. Organomet. Chem.* **2022**, *36* (1), No. e6466.

(45) Al-Ayash, S. R.; Al-Noor, T. H.; Abdou, A. Synthesis and Characterization of Metals Complexes with Uracil and Uracil Derivatives (A Review). *Russ. J. Gen. Chem.* **2023**, *93* (4), 987−995.

(46) Abdelazim, A. H.; Abourehab, M. A.; Abd Elhalim, L. M.; Almrasy, A. A.; Ramzy, S. Green adherent spectrophotometric determination of molnupiravir based on computational calculations; application to a recently FDA-approved pharmaceutical dosage form. *Spectrochimica Acta Part A: Molecular and Biomolecular Spectroscopy* **2023**, *285*, No. 121911.

(47) Abdou, A. Synthesis, structural, molecular docking, DFT, vibrational spectroscopy, HOMO-LUMO, MEP exploration, antibacterial and antifungal activity of new Fe (III), Co (II) and Ni (II) hetero-ligand complexes. *J. Mol. Struct.* **2022**, *1262*, No. 132911.

(48) Coats, A.; W. y Redfern, J. P. Kinetic Parameters from Thermogravimetric Data. *Nature (London)* **1964**, *201*, 68−69.

(49) Ge, J.; Wang, R.-q.; Liu, L. Study on the thermal degradation kinetics of the common wooden boards. *Procedia Engineering* **2016**, *135*, 72−82.

(50) Bansod, A.; Bhaskar, R.; Ladole, C.; Salunkhe, N.; Thakare, K.; Aswar, A. Synthesis, Characterization, Biological Activity and Solid-State Electrical Conductivity Study of Some Metal Complexes Involving Pyrazine-2-Carbohydrazone of 2-Hydroxyacetophenone. *J. Trans. Met. Compl.* **2022**, *5*, 1.

(51) Ismael, M.; Abdou, A.; Abdel-Mawgoud, A. M. Synthesis, Characterization, Modeling, and Antimicrobial Activity of FeIII, CoII, NiII, CuII, and ZnII Complexes Based on Tri-substituted Imidazole Ligand. *Z. Anorg. Allg. Chem.* **2018**, *644* (20), 1203−1214.

(52) Hrichi, H.; Elkanzi, N. A.; Ali, A. M.; Abdou, A. A novel colorimetric chemosensor based on 2-[(carbamothioylhydrazono) methyl] phenyl 4-methylbenzenesulfonate (CHMPMBS) for the detection of Cu (II) in aqueous medium. *Res. Chem. Intermed.* **2023**, *49* (5), 2257−2276.

(53) Abd El-Lateef, H. M.; Khalaf, M. M.; Kandeel, M.; Abdou, A. Synthesis, Characterization, DFT, Biological and Molecular Docking of Mixed Ligand Complexes of Ni (II), Co (II), and Cu (II) Based on Ciprofloxacin and 2-(1H-benzimidazol-2-yl) phenol. *Inorg. Chem. Commun.* **2023**, *155*, No. 111087.

(54) Shaaban, S.; Al-Faiyz, Y. S.; Alsulaim, G. M.; Alaasar, M.; Amri, N.; Ba-Ghazal, H.; Al-Karmalawy, A. A.; Abdou, A. Synthesis of New Organoselenium-Based Succinanilic and Maleanilic Derivatives and In Silico Studies as Possible SARS-CoV-2 Main Protease Inhibitors. *Inorganics* **2023**, *11* (8), 321.

(55) Jarad, A. J.; Dahi, M. A.; Al-Noor, T. H.; El-ajaily, M. M.; AL-Ayash, S. R.; Abdou, A. Synthesis, spectral studies, DFT, biological evaluation, molecular docking and dyeing performance of 1-(4-((2-amino-5-methoxy) diazenyl) phenyl) ethanone complexes with some metallic ions. *J. Mol. Struct.* **2023**, *1287*, No. 135703.

(56) Al-Wabli, R. I.; Resmi, K.S.; Sheena Mary, Y.; Yohannan Panicker, C.; Attia, M. I.; El-Emam, A. A.; Van Alsenoy, C. Vibrational spectroscopic studies, Fukui functions, HOMO-LUMO, NLO, NBO analysis and molecular docking study of (E)-1-(1, 3-benzodioxol-5-yl)-4, 4-dimethylpent-1-en-3-one, a potential precursor to bioactive agents. *J. Mol. Struct.* **2016**, *1123*, 375−383.

(57) Chaudhary, A. P.; Bharti, S. K.; Kumar, S.; Ved, K.; Padam, K. Study of molecular structure, chemical reactivity and first hyperpolarizability of a newly synthesized N-(4-oxo-2-phenylquinazolin-3 (4H)-yl)-1H-indole-2-carboxamide using spectral analysis. *J. Mol. Struct.* **2017**, *1148*, 356−363.

(58) El-Remaily, M. A. E. A. A. A.; El-Dabea, T.; El-Khatib, R. M.; Abdou, A.; El Hamd, M. A.; Abu-Dief, A. M. Efficiency and development of guanidine chelate catalysts for rapid and green synthesis of 7-amino-4,5-dihydro-tetrazolo[1,5-a]pyrimidine-6-carbonitrile derivatives supported by density functional theory (DFT) studies. *Appl. Organomet. Chem.* **2023**, *37* (11), No. e7262.

(59) Abd El-Lateef, H. M.; Khalaf, M. M.; Kandeel, M.; Amer, A. A.; Abdelhamid, A. A.; Abdou, A. New mixed-ligand thioether-quinoline complexes of nickel (II), cobalt (II), and copper (II): Synthesis, structural elucidation, density functional theory, antimicrobial activity, and molecular docking exploration. *Appl. Organomet. Chem.* **2023**, *37* (7), No. e7134.

(60) Shokr, E. K.; Kamel, M. S.; Abdel-Ghany, H.; El-Remaily, M. A. E. A. A. A.; Abdou, A. Synthesis, characterization, and DFT study of linear and non-linear optical properties of some novel thieno [2, 3-b] thiophene azo dye derivatives. *Mater. Chem. Phys.* **2022**, *290*, No. 126646.

(61) Jeba Reeda, V.S.; Bena Jothy, V.; Asif, M.; Nasibullah, M.; Alharbi, N. S.; Abbas, G.; Muthu, S. Synthesis, solvent polarity (polar and nonpolar), structural and electronic properties with diverse solvents and biological studies of (E)-3-((3-chloro-4-fluorophenyl) imino) indolin-2-one. *J. Mol. Liq.* **2023**, *380*, No. 121709.

(62) Abdelaziz, A.; Gaber, M.; El-Wakiel, N.; El-Sayed, Y. S. Ag (I), In (III), and Sn (II) chelates of azo mesalamine drug: Characterization, DFT studies, molecular docking and biological evaluation. *Appl. Organomet. Chem.* **2023**, *37* (2), No. e6944.

(63) Abbas, O. A.; El-Roudi, O. M.; Abdel-Latif, S. A. Novel 1, 3-diphenyl-4-(N, N-dimethylimido dicarbonimidic diamide azo)-5-pyrazolone and its chelates with manganese, nickel, copper, and zinc divalent metal ions as an antibacterial activity supported by molecular docking studies: Design, synthesis, DFT, and TD-DFT/PCM calculations. *Appl. Organomet. Chem.* **2023**, *37*, No. e7236.

(64) Martemucci, G.; Costagliola, C.; Mariano, M.; D'andrea, L.; Napolitano, P.; D'Alessandro, A. G. Free radical properties, source and targets, antioxidant consumption and health. *Oxygen* **2022**, *2* (2), 48−78.

(65) Gulcin, İ.; Alwasel, S. H. DPPH radical scavenging assay. *Processes* **2023**, *11* (8), 2248.

(66) Kareem, M. J.; Al-Hamdani, A. A. S.; Ko, Y. G.; Al Zoubi, W.; Mohammed, S. G. Synthesis, characterization, and determination antioxidant activities for new Schiff base complexes derived from 2-(1H-indol-3-yl)-ethylamine and metal ion complexes. *J. Mol. Struct.* **2021**, *1231*, No. 129669.

(67) Mohapatra, R. K.; Mahal, A.; Ansari, A.; Kumar, M.; Guru, J. P.; Sarangi, A. K.; Abdou, A.; Mishra, S.; Aljeldah, M.; AlShehail, B. M.; Alissa, M.; Garout, M.; Alsayyah, A.; Alshehri, A. A.; Saif, A.; Alqahtani, A.; Alshehri, F. A.; Alamri, A. A.; Rabaan, A. A. Comparison of the binding energies of approved mpox drugs and phytochemicals through molecular docking, molecular dynamics simulation, and ADMET studies: An in silico approach. *Journal of Biosafety and Biosecurity* **2023**, *5* (3), 118−132.

(68) El-Saghier, A. M.; Abdou, A.; Mohamed, M. A.; Abd El-Lateef, H. M.; Kadry, A. M. Novel 2-Acetamido-2-ylidene-4-imidazole Derivatives (El-Saghier Reaction): Green Synthesis, Biological Assessment, and Molecular Docking. *ACS omega* **2023**, *8* (33), 30519−30531.